

**Mean-field theory of ferroelectricity in  $\text{Sr}_{1-x}\text{Ca}_x\text{TiO}_3$  ( $0 \leq x \leq 0.4$ )**Y. J. Guo,<sup>1,2</sup> Y. Y. Guo,<sup>1</sup> L. Lin,<sup>1</sup> Y. J. Gao,<sup>2</sup> B. B. Jin,<sup>1</sup> L. Kang,<sup>1</sup> and J.-M. Liu<sup>1,3,\*</sup><sup>1</sup>Laboratory of Solid State Microstructures, Nanjing University, Nanjing 210093, China<sup>2</sup>Department of Physics, Jiangsu Institute of Education, Nanjing 210013, China<sup>3</sup>Institute for Advanced Materials, South China Normal University, Guangzhou 510006, China

(Received 13 May 2012; revised manuscript received 26 June 2012; published 10 July 2012)

A mean-field theory based on a modified transverse-field Ising model including the multifold interactions in  $\text{Sr}_{1-x}\text{Ca}_x\text{TiO}_3$  over a broad composition range from  $x = 0.0$  to  $0.4$  is developed and the full-scale phase diagram consistent with experiments is evaluated. In this theory, both the ferroelectric distortion and antiferrodistortive effects induced by  $\text{Ca}^{2+}$  substitution of  $\text{Sr}^{2+}$  are taken into account. It is revealed that the competition between those two types of lattice distortion effects plus the quantum fluctuations represent the core physics underlying the whole set of characteristics in  $\text{Sr}_{1-x}\text{Ca}_x\text{TiO}_3$  up to  $x = 0.4$ . The quantum fluctuations dominant state (quantum paraelectric state), ferroelectrically distorted state, and antiferrodistortive state are successfully predicted, upon increasing substitution level  $x$ . It is also predicted that the antiferrodistortive state in the high substitution level is the origin of antiferroelectric order which eventually suppresses the ferroelectric state.

DOI: [10.1103/PhysRevB.86.014202](https://doi.org/10.1103/PhysRevB.86.014202)

PACS number(s): 77.22.-d, 77.80.bj

**I. INTRODUCTION**

Perovskite structure  $ABO_3$ -type  $\text{SrTiO}_3$  (STO) and a series of oxides originated from STO by substitution have drawn substantial attention in the past decades for their peculiar critical phenomena and controllable quantum phase transitions.<sup>1-4</sup> Recently, quite a few application potentials for these STO-based materials in cryogenic electronics have been proposed too.<sup>5-9</sup> For STO which is a well-known quantum paraelectric (QPE) system, quantum fluctuations (QFs) play a decisive role in determining these phenomena and properties related to application potentials. It is understood that the manipulation of the distribution of atomic displacement in STO by QFs suppresses possible ferroelectric (FE) ordering over the whole temperature ( $T$ ) range and leads to a high and broad dielectric plateau instead of a dielectric peak representing the paraelectric-FE phase transition in the low- $T$  range.<sup>8</sup>

Besides intensive works on STO itself, substantial attention also goes to those STO-based materials and the most often addressed two systems are  $\text{Sr}_{1-x}\text{Ba}_x\text{TiO}_3$  (SBT) and  $\text{Sr}_{1-x}\text{Ca}_x\text{TiO}_3$  (SCT), both of which are synthesized by substitution of Sr at the A site of the perovskite structure while the chemistry of the  $\text{TiO}_6$  octahedral remains unaffected. Nevertheless, such an A-site substitution, even at low level, would generate tremendous and attractive changes in the structure and property. The  $\text{Ba}^{2+}$  (or  $\text{Ca}^{2+}$ ) ions have different ionic radius from  $\text{Sr}^{2+}$  ions, and the lattice distortion due to the substitution causes a series of effects and the primary one is the reentrant electric dipole ordering. Certainly, the Ba substitution is different from the Ca substitution in terms of the structural distortion and related properties. For SBT, electrical quadrupole moments are generated by the lattice distortion which is due to much larger  $\text{Ba}^{2+}$  ions (0.135 nm) than  $\text{Sr}^{2+}$  ions (0.118 nm), and these moments interact with each other and eventually the FE ordering is developed once  $x$  is higher than a low threshold value.<sup>9-15</sup> Although relaxor ferroelectric (RFE) like behaviors were reported in SBT with  $x$  lower than this threshold, no other attractive feature has been addressed, and the QPE state and FE state are the so far identified two ground states in SBT upon substitution level  $x$ .

However, the as-induced effect in SCT seems to be much more complicated. The substitution of  $\text{Sr}^{2+}$  by smaller  $\text{Ca}^{2+}$  (0.100 nm) leads to certain off-center ionic displacement in the tilted- $\text{TiO}_6$  octahedron which allows SCT to be substantially different from SBT.<sup>16-24</sup> As early as in 2000, Ranjan *et al.*<sup>18</sup> investigated in detail the structure and electric properties of SCT and evaluated a comprehensive phase diagram over a broad range  $0.0 \leq x \leq 0.4$ . This phase diagram is more complicated than that of SBT and the major characteristics are highlighted below [see Fig. 7(b)]. First, within  $0.0 \leq x \leq 0.016$ , SCT undergoes a phase transition from the QPE phase to quantum ferroelectric (QFE) phase at  $x = x_c \sim 0.002$ . This behavior is similar to SBT although the value of  $x_c$  is slightly different. Second, in the range  $0.016 < x \leq 0.12$ , SCT seems to be in the FE or RFE state and the transition point  $T_c$  is nearly independent of  $x$ .<sup>18,19</sup> Third, in the range  $0.12 < x \leq 0.2$ , no FE hysteresis can be observed and the anomalies in the dielectric susceptibility were argued to originate from an unknown phase transition into a cubic structure.<sup>18,24</sup> Fourth, an antiferroelectric (AFE) phase rather than the FE phase appears in the range  $0.2 < x \leq 0.4$ . This anomalous AFE phase is believed to originate from the antiferrodistortive (AFD) effect.<sup>8,18</sup> This complicated and composition-sensitive phase diagram raises substantial challenge to our understanding of the physics embedded in SCT.

In fact, this challenge has been addressed in recent years by extensive investigations from various aspects. Each of those observed states appearing in respective substitution ranges was once discussed. The quantum phase transition from the QPE state to the QFE state in the low- $x$  range is believed to be relevant to the polarized clusters centered at the  $\text{CaTiO}_3$  unit (CTO) and the interactions between these clusters are responsible for the long-range dipole ordering.<sup>19</sup> The FE- or RFE-like behaviors in the intermediate- $x$  range are the consequence of the dipole ordering or dipole frustration due to the  $\text{Ca}^{2+}$  substitution.<sup>18,24</sup> At relatively high  $x$ , the AFE state is believed to be linked with the opposite tilting of the  $\text{TiO}_6$  octahedra in neighboring CTO unit cells.<sup>18</sup> These contributions explain reasonably these different states respectively, but they originate from different mechanisms.

So far, however, no successful general theory which can predict all these states and their intertransitions over the whole substitution range has been available. Such a general theory allows us to understand these intertransitions in response to substitution in a unified framework and it is thus of special significance.

In this article, we are going to address this issue. It is well known that the transverse-field Ising model is a powerful approach to describe the quantum phase transitions and QFs in quantum paraelectrics and emergent FE systems.<sup>10,12,15,19</sup> The major motivation in dealing with SCT over a broad substitution range is to take into account the interactions between the polarized clusters in SCT over the high- $x$  range, which would bring substantial complexity mathematically. We present our strategy for a general mean-field theory based on our delicate analysis on possible mechanisms induced by the Ca substitution. Consequently, we propose a modified transverse-field Ising model and mean-field approximation. Based on it, a series of dielectric and FE properties as a function of the Ca-substitution are calculated. It will be shown that the calculated phase diagram for SCT fits quite well with the experimentally evaluated one and we demonstrate that the competitions between the QFs, FE order, and AFD effect represent the core physics underlying the phase diagram of SCT.

## II. TRANSVERSE-FIELD ISING MODEL

### A. Conventional transverse-field Ising model for doped STO

The conventional transverse-field Ising model (TIM) describing the quantum phase transitions of STO and related substituted systems takes the following Hamiltonian:<sup>10</sup>

$$\begin{aligned}
 H = & - \sum_{(i)} \Omega_{hi} s_{hi}^x - \sum_{(ij)} J_{ij}^{hh} s_{hi}^z s_{hj}^z - \sum_{(i)} \mu_i^h E_i s_{hi}^z \\
 & - \sum_{(i)} \Omega_{di} s_{di}^x - \sum_{(ij)} J_{ij}^{hd} s_{hi}^z s_{dj}^z - \sum_{(i)} \mu_i^d E_i s_{di}^z, \quad (1)
 \end{aligned}$$

where superscripts and subscripts ( $h, d$ ) refer to the host (STO) cells and dopant [BaTiO<sub>3</sub> (BTO) or CTO] cells, parameter  $s_i^x$  ( $s_i^z$ ) is the  $x$  ( $z$ ) component of pseudospin at site  $i$ ,  $\Omega_{hi}$  and  $\Omega_{di}$  are the individual tunneling frequencies of the host and dopant pseudospins at site  $i$ , respectively,  $J_{ij}^{hh}$  and  $J_{ij}^{hd}$  are the interactions between the host-host and host-dopant pseudospins, respectively,  $\mu_i^h$  and  $\mu_i^d$  are the effective dipolar moments of pseudospins  $s_{hi}^z$  and  $s_{di}^z$ , respectively, and  $E_i$  is the external electrical field. Usually,  $\Omega_{hi}$  and  $\Omega_{di}$ ,  $J_{ij}^{hh}$  and  $J_{ij}^{hd}$ , and  $\mu_i^h$  and  $\mu_i^d$  are treated as constants  $\Omega_h$  and  $\Omega_d$ ,  $J^{hh}$  and  $J^{hd}$ , and  $\mu^h$  and  $\mu^d$ . It is clearly seen that this TIM model applies to the cases of low substitution level since no dopant-dopant pseudospin interaction is considered.

In this model, the tunneling frequencies ( $\Omega_h$  and  $\Omega_d$ ) measure the magnitudes of zero-point QFs, while the pseudospin interaction ( $J^{hh} > 0$  and  $J^{hd} > 0$ ) would favor the FE order. Therefore, the ground state is determined by the competition between the QFs and FE ordering. For the host STO cell, the QFs are dominant so one has the tunneling ratio  $2\Omega_h/ZJ^h > 1$  (here  $Z$  denotes the number of the neighboring pseudospins). Therefore, the QPE state is the ground state. For the dopant

BTO or CTO cell, the ratio  $2\Omega_d/ZJ^d < 1$  and the QFs will be suppressed by the FE order as long as  $x$  is above a threshold value. In the framework of this TIM, the competition between the QFs (parameter  $\Omega$ ) and FE order (parameter  $J$ ) determines which of the QPE state and FE state is dominant. This is the well-known physics for understanding the QFs and FE order in both SBT and SCT.

Nevertheless, this model seems insufficient to explain all the complicated behaviors in SCT. For example, the AFE state associated with the AFD effect at higher  $x$  cannot be predicted. In fact, the Ca substitution would induce the off-center displacement, which on the other hand distorts the host cell lattice, and thus the CTO-centered polarized clusters would appear around the dopant sites. If the substitution level is very low, the dopant ions are spatially separated and thus the interdopant correlation is negligible if any and the dopant-induced polarized clusters do not overlap with each other. This overlap would become more probable when  $x$  increases. As long as the density of the polarized clusters reaches a critical value so that the overlapping occurs, a macroscopic polarization is expected, giving rise to a quantum phase transition from the QPE state to the normal FE state. However, further increasing of  $x$  would lead to the neighboring of these dopant cells and thus the interdopant interaction can no longer be negligible, which must be taken into account in the high- $x$  range.

It will be shown that this interaction is the core physics for understanding the AFD effect in SCT, which is also influential on other phenomena associated with the complicated phase transitions in SCT. The critical value of  $x$  above which this interaction has to be taken is  $\sim 0.016$ .

### B. Modified transverse-field Ising model for SCT

The nature of lattice distortion and phase transitions of SCT in the high- $x$  range is not yet clear, especially for the AFE state within  $0.2 \leq x \leq 0.4$ . For STO, it is well known that an AFD transition occurs at  $T \sim 105$  K, at which the high- $T$  simple cubic perovskite structure distorts into a tetragonal structure where the neighboring two tilted-TiO<sub>6</sub> octahedra rotate in opposite directions.<sup>8</sup> This collective rotation is called the zone boundary mode (i.e., AFD mode). In SCT, similar AFD octahedral rotations were also identified, which is hybridized with the FE distortion. As predicted in Ref. 22, the Ca<sup>2+</sup> distribution determines the rotation of oxygen cages accompanied with a displacement along the  $c$  axis. Therefore, it can be argued that the Ca-substitution-induced lattice distortion causes not only the zone center polar soft mode but probably the AFD mode.

This AFD mode can be schematically illustrated in Fig. 1 with two types of dopant occupancy as an example. Figure 1(a) shows an isolated CTO unit cell surrounded by host STO cells, which is called case I hereafter. The other case (case II) is shown in Fig. 1(b), where two neighboring CTO unit cells are considered as an example. Due to the smaller radius of Ca<sup>2+</sup> than Sr<sup>2+</sup>, Ca<sup>2+</sup> in a CTO cell would take a certain off-center displacement, which induces the tilting of the TiO<sub>6</sub> octahedra. As shown in Fig. 1(a), the tilting of the TiO<sub>6</sub> octahedra is relevant to the polarized cluster at the dopant site, and the long-range interaction between these polarized clusters may

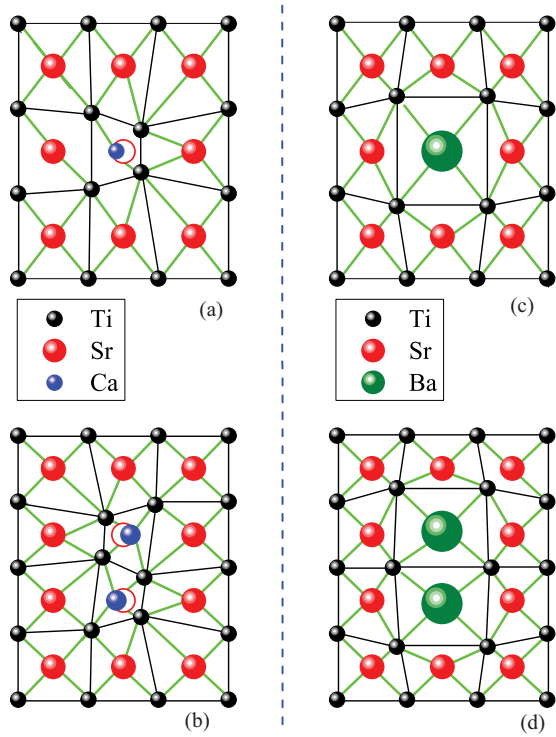


FIG. 1. (Color online) Sketch graphs for lattice distortions in Ca-substituted and Ba-substituted STO lattice. (a) A CTO cell surrounded with polarized cluster in case I. (b) Two neighboring CTO cells with the  $\text{TiO}_6$  octahedra tilted in opposite directions in case II. (c) A BTO cell and (d) two neighboring BTO cells in the lattice for comparison with (a) and (b).

induce the FE order. However, as shown in Fig. 1(b), the two neighboring  $\text{TiO}_6$  octahedra may also intend to rotate in opposite direction so as to maintain the stability of the lattice, i.e., an energy minimum. Such opposite tilted- $\text{TiO}_6$  octahedra rotation can be seen as a local AFD effect, which is approached by an interaction between two neighboring dopant pseudospins ( $J^{dd} < 0$ ) in our modified TIM, which would induce an antipolar cluster in the neighboring CTO cells. Similarly to  $\text{Ca}^{2+}$ , two types of  $\text{Ba}^{2+}$  occupancy are shown in Figs. 1(c) and 1(d). Due to larger radius of  $\text{Ba}^{2+}$  than  $\text{Sr}^{2+}$ ,  $\text{Ba}^{2+}$  in a BTO cell would induce an electrical quadrupole moment instead of an off-center displacement, and the opposite tilted- $\text{TiO}_6$  octahedra rotation would not appear. Therefore, no AFD effect in SBT is possible, even in the high- $x$  range. Surely, it should be pointed out that not all of the neighboring  $\text{TiO}_6$  octahedra pairs always tilt in opposite directions. Depending on the lattice configuration and competition between various energy terms, some of the neighboring  $\text{TiO}_6$  octahedra pairs may tilt in the same direction in spite of  $J^{dd} < 0$ . In this case, the  $\text{TiO}_6$  octahedra pair contributes to the zone center polar soft mode, i.e., the FE distorted mode.

As an approximation, at low- $x$  level, case I is dominant and the density of isolated CTO cells increases linearly with  $x$ , leading to the FE ordering. The AFD effect associated with case II becomes gradually significant at high- $x$  level, leading to the AFE ordering over the FE ordering. The Hamiltonian is

rewritten as

$$H = - \sum_{(i)} \Omega_{hi} s_{hi}^x - \sum_{(ij)} J_{ij}^{hh} s_{hi}^z s_{hj}^z - \sum_{(i)} \mu_i^h E_i s_{hi}^z - \sum_{(i)} \Omega_{di} s_{di}^x - \sum_{(ij)} J_{ij}^{hd} s_{hi}^z s_{dj}^z - \sum_{(i)} \mu_i^d E_i s_{di}^z - \sum_{(ij)} J_{ij}^{dd} s_{di}^z s_{dj}^z, \quad (2)$$

where  $J^{dd}$  is the interaction between the dopant pseudospins, and the only difference between Eq. (2) and Eq. (1) is the last term on the right of Eq. (2). Here  $J^{dd} < 0$  is assumed, favoring the antipolar alignment between two neighboring CTO cells.

The configuration  $\langle ij \rangle$  in Eq. (2) refers to the interactions between one pseudospin and its  $q$  neighbors. In the three-dimensional (3d) cubic lattice,  $q = 6$  if only the nearest neighbors are considered, and  $q = 18$  if the next-nearest neighbors are also included. This implies that for one dopant pseudospin, if one or more of its  $q$  neighbors are also dopant ones, the local AFD effect becomes possible. In the present model, the pseudospin interaction over the longer distance is neglected.

### C. Mean-field theory

Now we consider an  $N$ -pseudospin 3d lattice, where the numbers of dopant and host pseudospins are  $n_d = Nx$  and  $n_h = N(1-x)$ , respectively. We also assume that the CTO unit cells distribute randomly in the host STO lattice. For case I, every dopant pseudospin has  $q$  host pseudospin neighbors. The probability for finding this configuration is  $(1-x)^q$ . For the other case, case II, one dopant pseudospin must have at least one dopant pseudospin neighbor of its  $q$  neighbors. The probability for finding this configuration is  $1 - (1-x)^q$ . The numbers of the dopant pseudospins fitting the two cases are  $n_d(\text{I})$  and  $n_d(\text{II})$ :

$$n_d(\text{I}) = Nx(1-x)^q, \quad n_d(\text{II}) = Nx[1 - (1-x)^q]. \quad (3)$$

The number of CTO unit cells is thus the sum of  $n_d(\text{I})$  and  $n_d(\text{II})$ . Obviously, the number of inter-pseudospin bonds is  $f = Nq/2$ , which can be subdivided into four types: (i) the host-host bond and its number is  $f_{hh} = Nq(1-x)^2/2$ , (ii) the host-dopant bond in case I and its number is  $f_{hd}(\text{I}) = Nqx(1-x)^q$ , (iii) the host-dopant bond in case II and its number is  $f_{hd}(\text{II}) = Nqx[1 - (1-x)^q] - Nqx^2$ , and (iv) the dopant-dopant bond in case II and its number is  $f_{dd} = Nqx^2/2$ . In total, we have  $f = f_{hh} + f_{hd}(\text{I}) + f_{hd}(\text{II}) + f_{dd}$ .

To proceed, a mean-field approximation (MFA) is presented to obtain the solution to Eq. (2). Four order parameters are defined in this MFA scenario, denoted as  $\langle s_h \rangle$ ,  $\langle s_I \rangle$ ,  $\langle s_{IIA} \rangle$ , and  $\langle s_{IIB} \rangle$ , counting the numbers of the four types of pseudospins in this scenario.  $\langle s_h \rangle$  and  $\langle s_I \rangle$  represent the averages over the host pseudospins and dopant ones in case I, respectively.  $\langle s_{IIA} \rangle$  and  $\langle s_{IIB} \rangle$  are the averages over the dopant pseudospins in case II, while subscripts  $A$  and  $B$  denote respectively the two neighboring CTO unit cells in which the two tilted- $\text{TiO}_6$  octahedra would rotate. If  $\langle s_{IIA} \rangle$  and  $\langle s_{IIB} \rangle$  have the same sign, the corresponding two tilted- $\text{TiO}_6$  octahedra rotate in the same direction; otherwise they rotate in opposite directions. The relevant interactions are expressed as the corresponding effective fields. As a good approximation, one would see that  $|\langle s_{IIA} \rangle| \sim |\langle s_{IIB} \rangle|$ . Consequently, the effective fields for each

of the four order parameters can be written as

$$F_h = \left( \Omega_h, \quad 0, \quad 2\mu^h E + \frac{1}{n_h} \left[ 2f_{hh} J^{hh} \langle s_h \rangle + f_{hd}(\text{I}) J^{hd} \langle s_I \rangle + f_{hd}(\text{II}) J^{hd} \frac{\langle s_{IIA} \rangle + \langle s_{IIB} \rangle}{2} \right] \right), \quad (4a)$$

$$F_I = \left( \Omega_d, \quad 0, \quad 2\mu^d E + \frac{f_{hd}(\text{I})}{n_d(\text{I})} J^{hd} \langle s_h \rangle \right), \quad (4b)$$

$$F_{IIA} = \left( \Omega_d, \quad 0, \quad 2\mu^d E + \frac{2}{n_d(\text{II})} [f_{hd}(\text{II}) J^{hd} \langle s_h \rangle + f_{dd} J^{dd} \langle s_{IIB} \rangle] \right), \quad (4c)$$

$$F_{IIB} = \left( \Omega_d, \quad 0, \quad 2\mu^d E + \frac{2}{n_d(\text{II})} [f_{hd}(\text{II}) J^{hd} \langle s_h \rangle + f_{dd} J^{dd} \langle s_{IIA} \rangle] \right). \quad (4d)$$

Therefore, the self-consistent equations set for the four order parameters are

$$\langle s_\mu \rangle = \frac{F_\mu}{2|F_\mu|} \tanh \frac{|F_\mu|}{2k_B T}, \quad \mu = h, \text{I, IIA, IIB}, \quad (5)$$

where  $T$  is temperature and  $k_B$  the Boltzmann constant. Given a unit volume, polarization  $P$  can be expressed as the configuration summation over the four order parameters:

$$P = 2\mu^h n_h \langle s_h \rangle + 2\mu^d n_d(\text{I}) \langle s_I \rangle + \mu^d n_d(\text{II}) (\langle s_{IIA} \rangle + \langle s_{IIB} \rangle), \quad (6)$$

where  $N = 10^{30}/(3.905 - 0.1x)^3$ , suggesting the pseudospin density modified by the dopant.<sup>12,19</sup> The dielectric susceptibility is thus written as

$$\varepsilon = \frac{1}{\varepsilon_0} \frac{dP}{dE} \approx \frac{1}{\varepsilon_0} \frac{\Delta P}{\Delta E} = \frac{1}{\varepsilon_0} \frac{P(E = E_0) - P(E = 0)}{E_0}, \quad (7)$$

where  $E_0$  is a small electrical field (e.g.,  $E_0 = 1.0$  V/mm or less).

### III. RESULTS AND DISCUSSION

We perform extensive calculations on the competing QFs, FE distortion, and AFD effect in SCT from Eq. (6) and Eq. (7), and compare the calculated results with experimental phase diagram. In our calculation,  $q = 18$  is chosen to account for the next-neighboring pseudospin interaction in a 3d lattice. Other parameters for the calculation are listed in Table I, while their values are chosen referring to previous work on the TIM.<sup>9,12,15,17,18</sup> These parameters were carefully chosen to make the calculations be possibly consistent with experiments.

It will be shown that four regions in the substitution level can be distinguished in terms of the dielectric and ferroelectric behaviors. In region I,  $0.0 \leq x \leq 0.016$ , SCT undergoes a phase transition from the QPE state to the QFE state, while a FE or REF-like behavior is predicted in region II with  $0.016 < x \leq 0.12$ . In region III,  $0.12 < x \leq 0.2$ , a transition from the FE state to the AFD state is illustrated, and the AFE state

TABLE I. Parameters chosen for transverse-field Ising model.

$J^{hd}$ ( $k_B\text{K}$ )	32	$J^{dd}$ ( $k_B\text{K}$ )	-95	$J^h$ ( $k_B\text{K}$ )	9
$\Omega_h$ ( $k_B\text{K}$ )	86	$\Omega_d$ ( $k_B\text{K}$ )	86	$q$	18
$\mu^h$ ( $e\text{\AA}$ )	1.89	$\mu^d$ ( $e\text{\AA}$ )	2.95		

rather than the FE phase appears in region IV,  $0.2 \leq x \leq 0.4$ . Eventually, the experimentally measured phase diagram can be well reproduced and the possible phase structure in experimentally unknown region  $0.12 < x \leq 0.2$  is predicted.

#### A. Region I: $0 \leq x \leq 0.016$ , QPE to QFE phase transition

In Figs. 2(a) and 2(b), we present the calculated  $\varepsilon(T)$  and  $P(T)$  at  $x = 0.0, 0.008, 0.012$ , and  $0.016$ , respectively, while in Fig. 2(c), the four order parameters at  $x = 0.01$  as a function of  $T$  are presented. At  $x = 0$ , i.e., STO, no dielectric anomaly and nonzero  $P$  appear over the whole  $T$  range and a low- $T$  broad plateau of  $\varepsilon(T)$  is shown clearly, indicating the paraelectric state at high  $T$  and QPE state at low  $T$ . This result suggests that the QFs suppress the FE order and thus STO is a quantum paraelectrics. For  $x > 0$ , the FE ordering is gradually enhanced with increasing  $x$ , characterized by increasing FE Curie point  $T_c$  and enhanced saturated polarization  $P$ :  $T_c$  changes from 0 to  $\sim 26$  K and  $P$  changes from 0 to  $\sim 15$   $\mu\text{C}/\text{cm}^2$  as  $x$  increases from 0.0 to 0.0016. For each  $\varepsilon(T)$  and  $P(T)$  at  $x > 0$ , it is seen that the FE transition is typically second order and the  $\varepsilon(T)$  data above  $T_c$  can be roughly described by the Curie-Weiss law.

To illustrate the nature of the FE ordering, we plot the evaluated  $T_c$  (open square dots) as a function of  $x$ , as shown in Fig. 2(d). These data are fitted using the scaling formula  $T_c \sim (x - x_c)^\alpha$ , as given by the solid line, generating a scaling exponent  $\alpha = 0.497 \sim 1/2$  and a threshold value  $x_c = 0.0016$ . This threshold value is very close to experimentally identified value  $x_c \sim 0.002$ , while the scaling exponent  $\alpha \sim 1/2$  symbolizes a quantum phase transition. In this case, the system can be regarded as QFE phase.<sup>25,26</sup> It is thus indicated that SCT undergoes quantum phase transitions from the QPE phase to the QFE phase in the range  $0.0 \leq x \leq 0.016$ . While the upper boundary  $x = 0.016$  in terms of the FE ordering may not be very accurate, the data at  $x > 0.016$  begin to deviate from the scaling  $T_c \sim (x - x_c)^{1/2}$ .

In Fig. 2(c), order parameters are zero at  $T > T_c$ , while one has  $\langle s_I \rangle \gg \langle s_{IIA} \rangle = \langle s_{IIB} \rangle \gg \langle s_h \rangle$  below  $T_c$ , indicating that the largest contribution is from the CTO polarized clusters in case I and that from the STO polarized clusters is the smallest. It is noted that the equivalent  $\langle s_{IIA} \rangle$  and  $\langle s_{IIB} \rangle$  are positive, implying the almost identical contribution to the FE ordering from the two neighboring polarized clusters in case II and at the same time not any local AFD effect between the neighboring CTO cells is available. In fact, this is also reasonable since  $n_d(\text{II})$  is too small with respect to  $n_d(\text{I})$ , referring to Eq. (3).

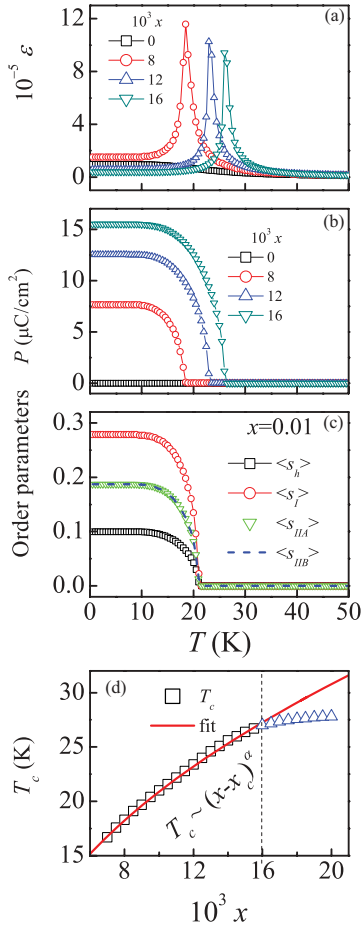


FIG. 2. (Color online) Calculated dielectric susceptibility  $\varepsilon(T)$  (a) and polarization  $P(T)$  (b) for several values of  $x$ , as well as the four order parameters as a function of  $T$  at  $x = 0.01$  (c), in region I:  $0.0 \leq x < 0.016$ . (d) Evaluated FE ordering point  $T_c$  as a function of  $x$ , with the calculated data (dots) and fitting (solid line) using the scaling relation  $T_c \sim (x - x_c)^{1/2}$ .

In short, the induced FE distortion is dominant in region I and the local AFD effect cannot be observable until  $x \sim 0.016$ . The scaling behavior in this region is mainly attributed to the competition between QFs and FE distortion arising from the CTO-centered polarized clusters.

### B. Region II: $0.016 < x \leq 0.12$ , normal FE phase

The calculated  $\varepsilon(T)$  and  $P(T)$  at  $x = 0.02, 0.04, 0.06$ , and  $0.10$ , respectively, are plotted in Figs. 3(a) and 3(b). In Fig. 3(c), the four order parameters as a function of  $T$  at  $x = 0.1$  are also presented. Similarly to region I, the FE transition in region II shows the second-order feature, and the FE order is further stabilized with increasing  $x$ , characterized by increasing  $T_c(x)$  and  $P(x)$ , as shown in Fig. 3(d). It is seen that  $T_c$  changes from 26 K to 44 K, and  $P$  varies from  $\sim 15 \mu\text{C}/\text{cm}^2$  to  $35 \mu\text{C}/\text{cm}^2$ . However, both  $T_c$  and  $P$  increase more slowly in region II ( $0.016 < x \leq 0.12$ ) than in region I ( $0 < x < 0.016$ ), and  $T_c(x)$  obviously deviates from the scaling behavior  $T_c \sim (x - x_c)^{1/2}$ , by which it can be argued that the FE state in region II is different from the QFE state in region I.

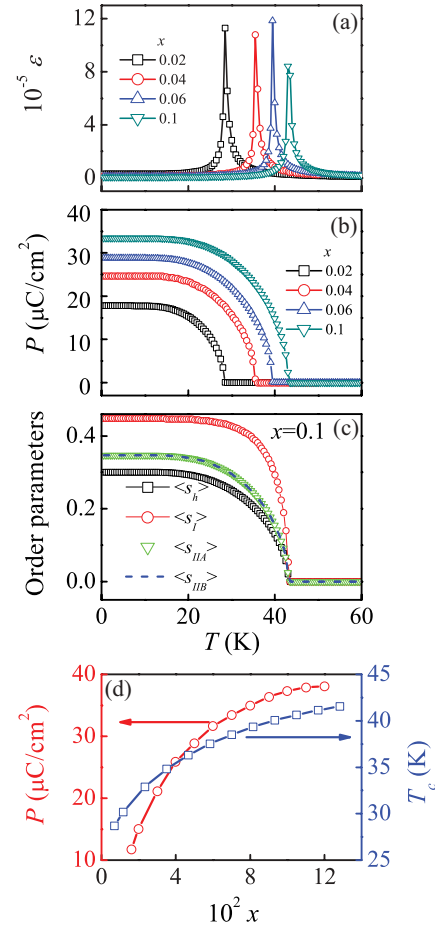


FIG. 3. (Color online) Calculated dielectric susceptibility  $\varepsilon(T)$  (a) and polarization  $P(T)$  (b) for several values of  $x$ , as well as the four order parameters as a function of  $T$  at  $x = 0.10$  (c), in region II:  $0.016 \leq x < 0.12$ . (d) Evaluated polarization  $P$  at  $T \sim 0$  K and FE ordering point  $T_c$  as a function of  $x$ .

It is quite challenging to identify the nature of the FE phase in region II. In fact, in this region the dielectric behavior above  $T_c$  still follows the Curie-Weiss law. On one hand, order parameter  $\langle s_I \rangle$  is larger than that in region I, and on the other hand order parameters  $\langle s_{IIA} \rangle$  and  $\langle s_{IIB} \rangle$  are much larger than those in region I too. It is noted that  $\langle s_{IIA} \rangle$  and  $\langle s_{IIB} \rangle$  are equivalent and both of them are positive, indicating higher densities of polarized clusters centered at both isolated single dopants and the nearest-neighboring dopants, which all favor the FE ordering and no AFD effect is available. Therefore, this region is mainly accommodated with FE state. However, it should be mentioned that in this region there still exist high-density single-dopant centered polarized clusters, implying the coexistence of these clusters with STO host phase. Therefore, the lattice here may not be typical FE state. Experimentally, the RFE-like behavior was identified in this region,<sup>27</sup> which should be related to this coexisting microstructure. In this sense, our prediction is consistent with experimental results, and a FE or RFE state is favored.

### C. Region III: $0.12 < x \leq 0.2$ , FE to AFD transition

Upon increasing of  $x$  over  $0.12$  until  $x = 0.2$ , the dielectric and FE behaviors show tremendous difference from those

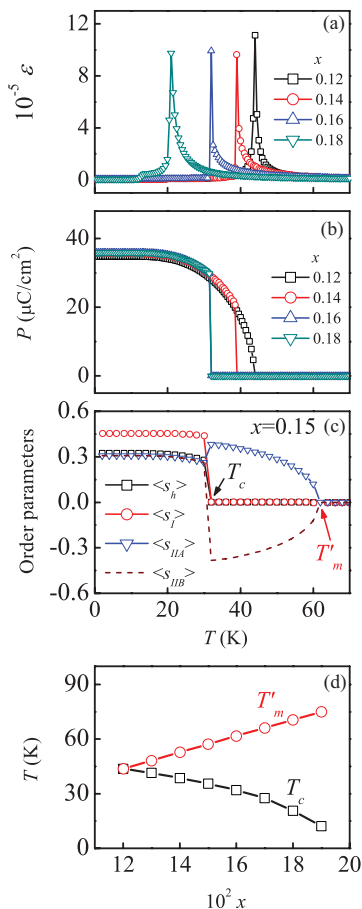


FIG. 4. (Color online) Calculated dielectric susceptibility  $\varepsilon(T)$  (a) and polarization  $P(T)$  (b) for several values of  $x$ , as well as the four order parameters as a function of  $T$  at  $x = 0.15$  (c), in region III:  $0.12 \leq x < 0.2$ . (d) Evaluated characteristic temperatures  $T_c$  and  $T'_m$  as a function of  $x$ .

observed in regions I and II. The  $\varepsilon(T)$  and  $P(T)$  data for several values of  $x$  ( $= 0.12, 0.14, 0.16$ , and  $0.18$ ) are presented in Fig. 4(a) and 4(b). First, the dielectric peak shifts to the low- $T$  range with increasing  $x$ , opposite to regions I and II where  $T_c$  increases with increasing  $x$ . Second, the  $P(T)$  data show an abrupt jump at  $T_c$ , consistent with the very sharp  $\varepsilon(T)$  peak. This suggests that the FE transition is of first order. To further illustrate the FE transitions here, as an example we plot the four order parameters as a function of  $T$  at  $x = 0.15$  in Fig. 4(c). Very different from regions I and II again, here order parameter  $\langle s_I \rangle$  ( $\langle s_h \rangle$ ) shows an abrupt jump from zero to a positive value at  $T_c$  where the first-order FE transitions occur. However, order parameters  $\langle s_{IIA} \rangle$  and  $\langle s_{IIB} \rangle$  experience the zero-to-nonzero transitions at a much higher  $T = T'_m$  than  $T_c$ , and then jumps at  $T_c$ . In particular, within  $T_c < T < T'_m$ ,  $\langle s_{IIA} \rangle$  and  $\langle s_{IIB} \rangle$  have opposite signs and similar magnitude to each other, indicating the AFD effect. Below  $T_c$ , both  $\langle s_{IIA} \rangle$  and  $\langle s_{IIB} \rangle$  become positive and equal to each other.

Based on the above data on  $\langle s_I(T) \rangle$ ,  $\langle s_{IIA}(T) \rangle$ , and  $\langle s_{IIB}(T) \rangle$ , one clearly sees an AFD transition initiating at  $T'_m$ , and then the AFD-FE transition at  $T_c$ . While the AFD phase is favored within  $T_c < T < T'_m$ , the ground state is still occupied by the FE phase, stating the competing FE distortion and AFD

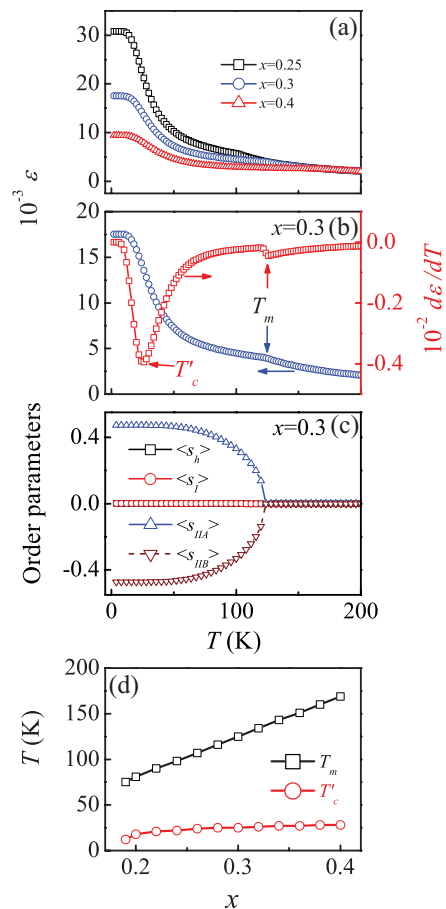


FIG. 5. (Color online) Calculated dielectric susceptibility  $\varepsilon(T)$  for several values of  $x$  (a),  $d\varepsilon(T)/dT$  at  $x = 0.30$  (b), as well as the four order parameters as a function of  $T$  at  $x = 0.30$  (c), in region IV:  $0.2 \leq x \leq 0.4$ . (d) Evaluated characteristic temperatures  $T'_c$  and  $T_m$  as a function of  $x$ .

effect in this region. A plotting of  $T'_m$  and  $T_c$  as a function of  $x$  is shown in Fig. 4(d), identifying the opposite  $x$  dependences of them:  $T_c$  is suppressed and  $T'_m$  is enhanced by the increasing CTO dopants, while they coincide with each other at  $x \sim 0.12$ . This also evidences the dominance of the FE distortion over the AFD effect at  $x \leq 0.12$ , making the latter negligible.

Experimentally, the nature of this region III remains unclear.<sup>18,24</sup> One of the major predictions of this work is that this is a FE-AFD competing region. The lattice experiences multiplied structure transition. The AFD distortion is dominant in the intermediate- $T$  range, and the ground state prefers the FE phase.

#### D. Region IV: $0.2 < x \leq 0.4$ , AFE phase

At  $x > 0.2$ , it comes to region IV. The calculated  $\varepsilon(T)$  data at  $x = 0.25, 0.3$ , and  $0.4$  are plotted in Fig. 5(a), respectively, while  $P(T) \sim 0.0$  over the whole  $T$  range, indicating no FE phase in this region. Taking one set of  $\varepsilon(T)$  data at  $x = 0.3$  as an example, as shown in Fig. 5(b), one sees clearly two anomalies at  $T_m$  ( $\sim 125$  K) and  $T'_c$  ( $\sim 25$  K), respectively, as identified more clearly by the  $d\varepsilon/dT$  as a function of  $T$ . The two  $\varepsilon(T)$  anomalies reflect two phase transitions. To proceed,

we consult the order parameters and the results at  $x = 0.3$  are plotted in Fig. 5(c). It is seen that both  $\langle s_l \rangle$  and  $\langle s_h \rangle$  are zero over the whole  $T$  range; however, nonzero  $\langle s_{IIA} \rangle$  and  $\langle s_{IIB} \rangle$  with  $\langle s_{IIA} \rangle = -\langle s_{IIB} \rangle$  at  $T < T_m$  appear and tend to be saturated values at low  $T$ . Therefore, the phase transition at  $T_m$  is associated with typical AFE ordering and  $T_m$  denotes the phase transition point from the AFE phase to paraelectric phase. It is also noted that  $\varepsilon(T)$  is about two orders of magnitude smaller than that for the FE phase, typical for the AFE phase.

In Fig. 5(d), the evaluated  $T_m$  and  $T'_c$  as a function of  $x$  are presented. Here,  $T_m$  represents the transition point of the AFE phase, which increases linearly with increasing  $x$ , while  $T'_c$  remains less dependent of  $x$  within this range. Unfortunately, no clear understanding of the phase transitions at  $T'_c$  is available to us. This event leads to a broad  $\varepsilon(T)$  plateau on the low- $T$  side, while no anomaly in the order parameters is observed. This allows an argument that this transition has not much to do with the AFD or FE mode. In a qualitative sense, with increasing  $n_d(\text{II})$ , the frustration of AFD effect between neighboring cells should be taken into consideration, which would cause the lattice to reenter into a QPE state, considering the fact that CTO crystal itself exhibits strong quantum fluctuations at low temperature,<sup>16</sup> and a similar anomaly was also observed in samples  $x = 0.35$  and  $0.40$ .<sup>18</sup>

### E. Phase diagram over $0.0 \leq x \leq 0.40$ and experimental relevance

Our calculation based on the modified transverse-field Ising model taking into account the CTO dopant-dopant interaction [Eq. (2)] clearly divides the whole Ca-substitution regime  $0.0 \leq x \leq 0.40$  into four regions. These results allow us to evaluate the phase diagram which can be compared with experimental data. We start from Eq. (3) to present  $n_d(\text{I})$  and  $n_d(\text{II})$  in Fig. 6, where the four regions are marked. This phase diagram in terms of the densities of isolated CTO dopant and those CTO dopants each having at least one neighboring dopant is also useful for us to understand the underlying physics for the Ca substitution. As discussed earlier,  $n_d(\text{I})$  is related to the FE distortion, and  $n_d(\text{II})$  scales the AFD effect. The phase transitions can be contributed to the variation of  $n_d(\text{I})$  and  $n_d(\text{II})$  with  $x$ , which determines the competition between the FE distortion and AFD effect. The dependencies of  $n_d(\text{I})$  and  $n_d(\text{II})$  on  $x$  show the one-to-one correspondence with the phase diagram to be given below.

The phase diagram in terms of the ordering parameters, evaluated from the above calculated data, is presented in Fig. 7(a), while we collect so far available experimental data to replot an experimental phase diagram,<sup>18,27</sup> as shown in Fig. 7(b). In a general sense, if no quantitative comparison is made, one finds quite good consistency between the calculated and experimental phase diagrams. Furthermore, the calculated results predict the nature of several phases which have not yet been identified experimentally, shedding light on further experimental investigation on the phase diagram in future. For instance, in region III, subsequent transitions from the high- $T$  PE phase to the AFD state and then to the FE phase with decreasing  $T$  are predicted. Such transitions become challenging experimentally using conventional electrical probing

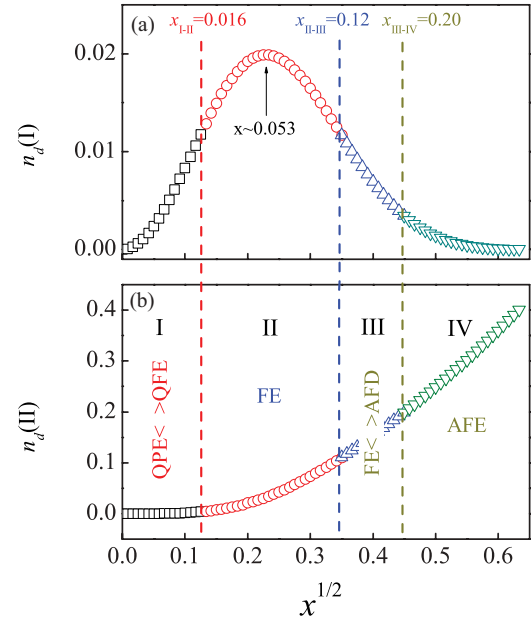


FIG. 6. (Color online) Calculated parameters  $n_d(\text{I})$  and  $n_d(\text{II})$  as a function of  $x$ , respectively. The four regions are separated by vertical lines and boundary values of  $x$ . PE: paraelectric phase; QPE: quantum paraelectric phase; QFE: quantum ferroelectric phase; FE: ferroelectric phase; RFE: relaxor ferroelectric phase; AFD: antiferrodistortive phase; AFE: antiferroelectric phase.

techniques, while direct probe of the local dipole configuration using neutron scattering would be required. Nevertheless, in the present mean-field theory, due to the limited order

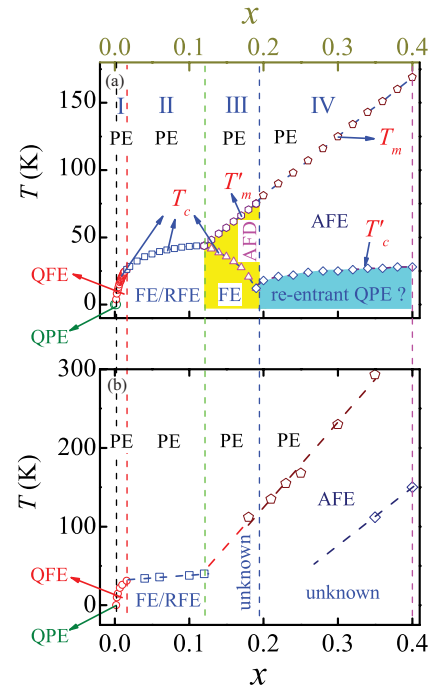


FIG. 7. (Color online) Calculated phase diagram (a) and measured phase diagram (b) for SCT over the composition range  $0 \leq x \leq 0.4$ . Data points marked by circles and squares correspond to Ref. 27; the pentagons and diamonds are taken from Ref. 18.

parameters, not every particular phase can be clearly revealed. For example, the ground state in region IV is vague. If it is a reentrant QPE phase, as claimed here, none of the four order parameters can characterize the phase transitions from the high- $T$  AFE phase. Therefore, additional physical ingredients should be taken into account for a more comprehensive treatment.

It should be addressed here that in a quantitative sense, good consistency between the calculated and measured results in regions I and II are shown, while such a consistency for regions III and IV is not. In particular, the measured transition points are two times higher than calculated ones, raising issues to be concerned for the present theory. We attribute this discrepancy to the mean-field approximation made in the model. One of the possible reasons for the discrepancy is that large antipolar domains centered at the dopant ions may form when the Ca substitution level is high. The domain wall energy from such structure would make the AFE phase more stable than the one predicted in our mean-field theory. Thus, the calculated transition temperature would be a little lower than the measured ones with increasing level  $x$ , especially from  $x > 0.2$ . In this sense, a quantitative prediction of the transition point at higher substitution level may not be reliable, unless additional interactions such as more than the next-nearest-neighboring ones and the crystalline anisotropy effect are taken into account. An inclusion of these interactions makes the mean-field approach quite challenging at this stage, even though the present model represents one of the comprehensive theories which reproduce most observed phenomena in the SCT system over a broad composition range.

#### IV. CONCLUSION

In conclusion, we have proposed a modified transverse-field Ising model and developed a general mean-field theory on the competition between FE ordering and the AFD effect plus the role of QFs in SCT over a broad composition range  $0 \leq x \leq 0.4$ . A phase diagram covering the phase transitions from the QPE state to the QFE state, then to the FE state, and eventually to the AFE state is calculated. The evaluated phase diagram shows good consistency with the measured phase diagram, although a quantitative fitting is not yet available in the high substitution level. The core physics, as revealed here, is the antipolar interaction between the neighboring dopant cells, representing the AFD effect, which competes with the FE ordering in the background of QFs, and consequently, the transitions from the QPE state to the AFE state via the intermediate QFE state, FE state, and AFD dominant state. The present theory represents a comprehension of the ferroelectric and antiferroelectric behaviors in SCT in various Ca-substitution ranges.

#### ACKNOWLEDGMENTS

This work was supported by the Natural Science Foundation of China (11104118, 11074113), the National Key Projects for Basic Research of China (2009CB623303, 2011CB922101), the China Postdoctoral Science Foundation (20110490130), the Jiangsu Postdoctoral Science Foundation of China (1101008B), and the Priority Academic Program Development of Jiangsu Higher Education Institutions, China.

\*Author to whom correspondence should be address: liujm@nju.edu.cn

<sup>1</sup>K. A. Müller and H. Burkard, *Phys. Rev. B* **19**, 3593 (1979).

<sup>2</sup>J. Hemberger, M. Nicklas, R. Viana, P. Lunkenheimer, A. Loidl, and R. Böhmer, *J. Phys.: Condens. Matter* **8**, 4673 (1996).

<sup>3</sup>Y. Yamada, N. Todoroki, and S. Miyashita, *Phys. Rev. B* **69**, 024103 (2004).

<sup>4</sup>M. I. Marqués, C. Aragón, and J. A. Gonzalo, *Phys. Rev. B* **72**, 092103 (2005).

<sup>5</sup>C. Filipič and A. Levstik, *Phys. Rev. B* **73**, 092104 (2006).

<sup>6</sup>R. Wahl, D. Vogtenhuber, and G. Kresse, *Phys. Rev. B* **78**, 104116 (2008).

<sup>7</sup>I. Katayama, H. Shimosato, D. S. Rana, I. Kawayama, M. Tonouchi, and Masaaki Ashida, *Appl. Phys. Lett.* **93**, 132903 (2008).

<sup>8</sup>W. Zhong and D. Vanderbilt, *Phys. Rev. B* **53**, 5047 (1996).

<sup>9</sup>L. Zhang, W. L. Zhong, and W. Kleemann, *Phys. Lett. A* **276**, 162 (2000).

<sup>10</sup>Y. G. Wang, W. Kleemann, W. L. Zhong, and L. Zhang, *Phys. Rev. B* **57**, 13343 (1998).

<sup>11</sup>V. B. Shirokov, V. I. Torgashev, A. A. Bakirov, and V. V. Lemanov, *Phys. Rev. B* **73**, 104116 (2006).

<sup>12</sup>H. Wu and W. Z. Shen, *Phys. Rev. B* **73**, 094115 (2006).

<sup>13</sup>T. Wei, Y. J. Guo, P. W. Wang, D. P. Yu, K. F. Wang, C. L. Lu, and J.-M. Liu, *Appl. Phys. Lett.* **92**, 172912 (2008).

<sup>14</sup>T. Wei, Y. Y. Guo, Y. J. Guo, S. J. Luo, K. F. Wang, J.-M. Liu, P. W. Wang, and D. P. Yu, *J. Phys.: Condens. Matter* **21**, 375901 (2009).

<sup>15</sup>Y. J. Guo, T. Wei, C. Zhu, K. F. Wang, X. S. Gao, Y. Q. Guan, and J.-M. Liu, *J. Appl. Phys.* **107**, 074106 (2010).

<sup>16</sup>J. G. Bednorz and K. A. Müller, *Phys. Rev. Lett.* **52**, 2289 (1984).

<sup>17</sup>W. Kleemann, J. Dec, Y. G. Wang, P. Lehnen, and S. A. Prosandeev, *J. Phys. Chem. Solids* **61**, 167 (2000).

<sup>18</sup>R. Ranjan, D. Pandey, and N. P. Lalla, *Phys. Rev. Lett.* **84**, 3726 (2000).

<sup>19</sup>L. Zhang, W. Kleemann, and W. L. Zhong, *Phys. Rev. B* **66**, 104105 (2002).

<sup>20</sup>G. Geneste and J.-M. Kiat, *Phys. Rev. B* **77**, 174101 (2008).

<sup>21</sup>S. K. Mishra and D. Pandey, *Appl. Phys. Lett.* **95**, 232910 (2009).

<sup>22</sup>A. Y. Kuksin, G. E. Norman, V. V. Pisarev, V. V. Stegailov, and A. V. Yanilkin, *Phys. Rev. B* **82**, 174101 (2010).

<sup>23</sup>T. Wei, J.-M. Liu, Q. J. Zhou, and Q. G. Song, *Phys. Rev. B* **83**, 052101 (2011).

<sup>24</sup>T. Mitsui and W. Westphal, *Phys. Rev.* **124**, 1354 (1961).

<sup>25</sup>V. V. Lemanov, E. P. Smirnova, P. P. Syrnikov, and E. A. Tarakanov, *Phys. Rev. B* **54**, 3151 (1996).

<sup>26</sup>W. Kleemann, J. Dec, and B. Westwanski, *Phys. Rev. B* **58**, 8985 (1998).

<sup>27</sup>I. S. Kim, M. Itoh, and T. J. Nakamura, *Solid State Chem.* **101**, 77 (1992).